First application of the n-^{9}Be optical potential to the study of the ^{10}Be continuum via the (^{18}O,^{17}O) neutron-transfer reaction

D. Carbone,[1,*] M. Bondì,[1,2] A. Bonaccorso,[3] C. Agodi,[1] F. Cappuzzello,[1,2] M. Cavallaro,[1] R. J. Charity,[4] A. Cunsolo,[1] M. De Napoli,[5] and A. Foti[2,5]

[1]*INFN, Laboratori Nazionali del Sud, Via S. Sofia 62, 95125 Catania, Italy*

[2]*Dipartimento di Fisica e Astronomia, Università di Catania, Via S. Sofia 64, 95125 Catania, Italy*

[3]*INFN, Sezione di Pisa, Largo Pontecorvo 3, 56127 Pisa, Italy*

[4]*Department of Chemistry, Washington University, St. Louis, Missouri 63130, USA*

[5]*INFN, Sezione di Catania, Via S. Sofia 64, 95125 Catania, Italy*

(Received 13 October 2014; published 24 December 2014)

The ^{9}Be(^{18}O,^{17}O)^{10}Be reaction has been studied at an incident energy of 84 MeV, and the ejectiles have been detected at forward angles. The ^{10}Be excitation energy spectrum has been obtained up to about 18 MeV, and several known bound and resonant states of ^{10}Be have been identified. Calculations that describe the interaction of the neutron removed from the ^{18}O projectile with the ^{9}Be target by means of an optical potential with a semiclassical approximation for the relative motion account for a significant part of the ^{10}Be continuum. Two parametrizations of the optical-model potential for the system n-^{9}Be have been used and compared.

DOI: 10.1103/PhysRevC.90.064621 PACS number(s): 25.70.Hi, 29.30.Ep, 25.60.Gc, 24.10.Ht

I. INTRODUCTION

Heavy-ion direct transfer reactions at energies just above the Coulomb barrier are worthy tools for obtaining precise spectroscopic information [1,2]. In particular, it was recently demonstrated that the (^{18}O,^{16}O) two-neutron transfer reaction is a powerful probe for quantitative spectroscopic studies of pair configurations in nuclear states [3]. The results presented in Ref. [3] belong to a systematic study, aiming at the investigation of one- and two-neutron excitations, which was started at the Catania Istituto Nazionale di Fisica Nucleare-Laboratori Nazionali del Sud (INFN-LNS) laboratories exploring the (^{18}O,^{17}O) and (^{18}O,^{16}O) one- and two-neutron transfer reactions. In this context, a fully quantum-mechanical approach, such as the distorted-wave Born approximation (DWBA) or the coupled reaction channel methods, would be the right framework to describe such reactions [4]. However, to date it has been impossible to calculate exactly the transfer to final continuum states due to the slow convergence of the numerical procedure. The problem originates from the fact that the final continuum wave functions extend to infinity and contain in principle a sum over an infinite number of partial waves. This problem is at present of particular importance because (d,p) reactions are often used to populate and study resonances of unbound nuclei at and beyond the neutron drip line (see, for example, Ref. [5]). On the other hand, semiclassical approaches have proven to be accurate enough to explain integral properties, such as the selectivity of the reaction, which allows one to also treat the transfer to bound and unbound states in a coherent way. In particular, in Ref. [6] it has been shown that different contributions to the reaction, such as elastic breakup and absorption from bound states and resonances of the target can be distinguished, at least for the case of one-neutron transfer. Within the same method, the problem of the convergence of the sum over partial waves has been solved. Furthermore, the model has also proven to be quantitatively successful in describing complicated spectra for transfer to the continuum reactions in which resonant and nonresonant contributions were involved [6,7]. Calculations of this kind, which assume an uncorrelated removal of the two neutrons, were recently performed to describe the continuum of ^{15}C and ^{14}C populated by (^{18}O,^{16}O) reactions [8,9]. These reactions were interpreted as a two-step mechanism as, for example, $^{18}\mathrm{O} + {}^{13}\mathrm{C} \rightarrow {}^{17}\mathrm{O} + {}^{14}\mathrm{C}_{\mathrm{g.s.}} \rightarrow {}^{16}\mathrm{O} + {}^{14}\mathrm{C}_{\mathrm{g.s.}} + n$ that starts from the one-neutron emission threshold (S_n) and $^{18}\mathrm{O} + {}^{13}\mathrm{C} \rightarrow {}^{17}\mathrm{O} + {}^{13}\mathrm{C}_{\mathrm{g.s.}} + n \rightarrow {}^{16}\mathrm{O} + {}^{13}\mathrm{C}_{\mathrm{g.s.}} + n + n$ that starts from the two-neutron emission threshold (S_{2n}). To perform such calculations it is important to know the optical potential, which, in the above-mentioned case, describes the $n + {}^{14}$C and $n + {}^{13}$C interaction. In Ref. [8] it was demonstrated that such an approach gives a good explanation of the continuum background in the ^{15}C spectrum, which shows an enhancement of the cross section just above the two-neutron emission threshold (S_{2n}).

Exploratory calculations were also developed for the ^{9}Be(^{18}O,^{16}O)^{11}Be reaction [10]. The ^{11}Be case is of particular interest since it is a neutron-rich nucleus where the detailed structure of its excited states is not well known. The semiclassical approach mentioned above can be useful to understand the contributions present in the ^{11}Be continuum spectrum populated by the (^{18}O,^{16}O) reaction. Therefore, the knowledge of the optical potentials that describe the n-^{10}Be and n-^{9}Be interactions are needed. Moreover, it is important to have a good description of the ^{9}Be(^{18}O,^{17}O)^{10}Be intermediate channel at the same incident energy, which enters in the description of the two-neutron transfer process.

In this paper we report on the study of the ^{10}Be continuum populated via the (^{18}O,^{17}O) one-neutron transfer reaction at an incident energy of 84 MeV. In a previous experiment, the reaction ^{9}Be(^{18}O,^{17}O)^{10}Be was studied at incident energies of 16 and 20 MeV, but only the transition to $^{10}\mathrm{Be}_{\mathrm{g.s.}}$ was

*Corresponding author: carboned@lns.infn.it

observed as those to the excited states of ^{10}Be were too weakly populated [11]. Two n-^{9}Be optical potentials, recently developed in Ref. [12], have been successfully employed here to describe the continuous part of the ^{10}Be spectra. They were constructed by fitting the n-^{9}Be total, elastic, and reaction cross sections measured in the free-neutron scattering over a large range of energies.

II. THE EXPERIMENT

The $^{18}O^{6+}$ beam, with incident energy of 84 MeV, was accelerated by the tandem Van de Graaff facility of INFN-LNS and bombarded a $130 \pm 6\,\mu g/cm^2$ self-supporting ^{9}Be target produced at the LNS chemical laboratory. A total charge of $31\,\mu C$ was integrated by a Faraday cup, downstream of the target. Supplementary runs with a $59 \pm 3\,\mu g/cm^2$ self-supporting ^{12}C target and a $212 \pm 10\,\mu g/cm^2$ WO_3 foil mounted on a $193 \pm 10\,\mu g/cm^2$ Au backing were recorded for estimating the background in the ^{10}Be energy spectrum coming from ^{12}C and ^{16}O impurities in the ^{9}Be target. The ^{17}O ejectiles were momentum analyzed by the MAGNEX spectrometer working in the full acceptance mode (solid angle $\Omega \sim 50$ msr and momentum range $\Delta p/p \sim 24\%$) [13,14]. The spectrometer was set for covering an angular range between 4° and 14° in the laboratory reference frame. The particle identification was performed by the simultaneous measurement of the angle and the position at the focal plane, the energy loss in the gas section of the focal plane detector [15] and the residual energy on the silicon detector hodoscope. Details about this technique can be found in Ref. [16].

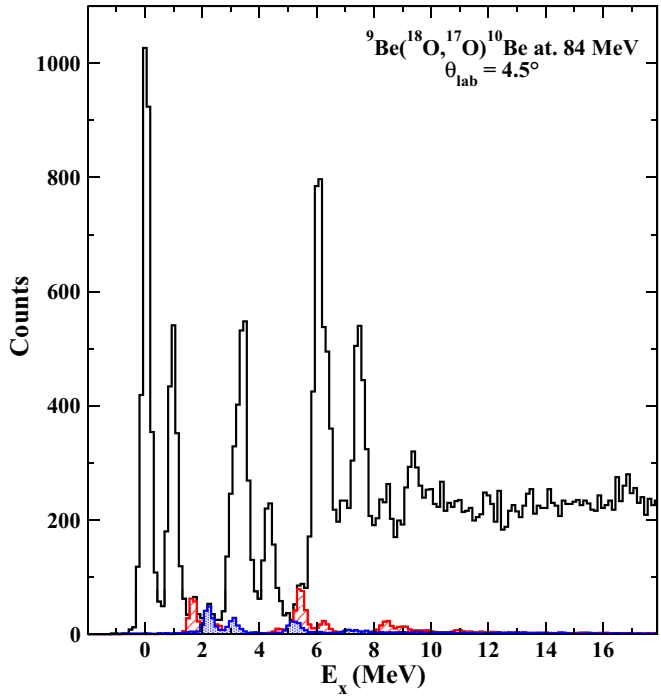

FIG. 1. (Color online) Excitation energy spectrum of the ^{9}Be(^{18}O,^{17}O)^{10}Be reaction at 84-MeV incident energy and $\theta_{lab} = 4.5°$. The background that comes from ^{12}C and ^{16}O impurities is shown as the blue-dotted and red-hatched areas, respectively.

To compensate the high-order aberrations connected with the large acceptance of the spectrometer, a tenth -order reconstruction of the scattering angle and momentum modulus was performed. This is based on the fully algebraic method implemented in MAGNEX [17,18] and needs the horizontal and vertical positions and angles at the focal plane as input. The excitation energies $E_x = Q_0 - Q$ [where Q_0 is the ground state (g.s.) Q value] were then obtained by the application of relativistic kinematic transformations. An overall energy and angular resolution of about 180 keV and 0.3°, respectively, were obtained. This was mainly determined by the straggling introduced by the target. The total error in the measured absolute cross section is about 10% induced by the uncertainties in the target thickness and beam integration. An example of the obtained energy spectra for the ^{10}Be residual nucleus is shown in Fig. 1 together with the contributions from the ^{12}C and ^{16}O impurities in the target, which are found to be small.

III. SPECTRUM DESCRIPTION

An example of the energy spectrum obtained after the subtraction of the contribution that arises from ^{12}C and ^{16}O impurities is shown in Fig. 2. Some narrow states of ^{10}Be are recognized below the one-neutron emission threshold

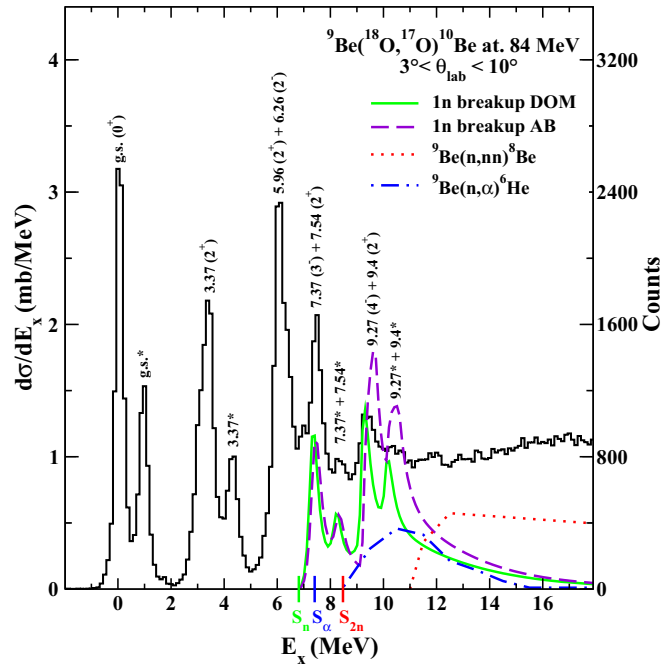

FIG. 2. (Color online) Inclusive excitation energy spectrum of the ^{9}Be(^{18}O,^{17}O)^{10}Be reaction at 84-MeV incident energy and $3° < \theta_{lab} < 10°$. The background that comes from ^{12}C and ^{16}O impurities has been subtracted. Peaks marked with an asterisk refer to the ^{17}O ejectile emitted in its first excited state at 0.87 MeV. Total $1-n$ breakup calculations that result from the use of the DOM and the AB potentials (see text) [12] are shown as the green-continuous and the violet-dashed lines, respectively. The experimental data [22] of the ^{9}Be(n,nn)^{8}Be [23] and ^{9}Be(n,α)^{6}He [24] reactions are reported as the red-dotted and blue-dotted-dashed lines, respectively. The $1n$-(S_n), $2n$-(S_{2n}), and α-(S_α) separation energies are also indicated.

($S_n = 6.812$ MeV), namely, the ground (0^+) and the excited states at $E_x = 3.37(J^\pi = 2^+), 5.96(1^-), 6.26(2^-)$ MeV. These are the same ^{10}Be bound states strongly populated in the (d,p) reactions on ^{9}Be [19,20]. However, there are some noticeable differences between the present experiment and those of Refs. [19,20]. When the transfer of the neutron happens from a deuteron, the neutron initial state is mainly an s state. Thus there is no enhancement due to the angular momentum coupling between initial and final states (see Ref. [21] for a quantitative discussion on this point). Also the incident energy was 8.6 A MeV in Ref. [19], whereas the beam energy used in the present case is 4.7 A MeV, which favors the population of the low-lying resonances.

In the energy spectrum shown in Fig. 2, each ^{10}Be state shows up as a doublet corresponding to the ^{17}O ejectile emitted in its ground and first excited states at $E_x = 0.87(1/2^+)$ MeV. The contribution of the higher ^{17}O excited states is less relevant and undistinguishable among the other peaks. Above the one-neutron emission threshold, there are two narrow peaks at ∼7.4 and ∼9.4 MeV. The first is identified as the superposition of the resonances at $E_x = 7.37(3^-), 7.54(2^+)$ MeV and the second of those at $E_x = 9.27(4^-), 9.40(2^+)$ MeV. A large background is present above ∼10 MeV of excitation energy, and no resonances are identified in this region. To understand what contributions are present in the region of the spectrum above the one-neutron emission threshold, the one-neutron continuum was studied by the transfer to the continuum model developed in Ref. [6].

IV. THEORETICAL DESCRIPTION

The cross section for one-neutron transfer between initial and final single-particle states can be calculated by using the model described in Refs. [25–28] in which it is given as a function of the final energy of the neutron in the continuum. This energy is connected to the kinetic energy of the ejectile, which is measured experimentally, by the energy-conservation relation,

$$E_x = E_{in} - E_f + Q_0 = \varepsilon_f + S_n,$$

where E_x is the targetlike excitation energy (i.e., ^{10}Be in the present case), E_{in} and E_f are the initial and final centers of mass energies, Q_0 is the ground state to ground state Q value, and ε_f is the final neutron energy. In the region of the spectra where $E_x > S_n$ the neutron final energy is positive and the transfer is populating continuum states. Here the experimental spectra are characterized by narrow resonances and bumps superimposed on a continuum background, which is mainly composed of elastic and nonresonant inelastic breakup contributions.

The model adopted for transfer reactions to a final state in the continuum is a generalization of a model for transfer between bound states [29–31]. The initial and final states are single-particle states, and it is assumed that the transfer is sensitive only to the tail of the wave functions, which are taken as Hankel functions. The projectile-target relative motion is treated semiclassically. The transfer probability from an initial bound state of definite energy ε_i, angular momentum l_i, and spin j_i to a final continuum state of positive energy ε_f is given by

$$\frac{dP}{d\varepsilon_f}(j_f, j_i) = \sum_{j_f} \left(\left|1 - \bar{S}_{j_f}\right|^2 + 1 - \left|\bar{S}_{j_f}\right|^2\right) B(j_f, j_i), \quad (1)$$

where $\bar{S}_{j_f}$ is the energy averaged and angular momentum-dependent optical model S matrix, which describes the rescattering of the neutron on the target, and $B(j_f, j_i)$ is the elementary transfer probability. The latter depends on the details of the initial and final states, on the energy of the relative motion, and on the distance of closest approach between the two nuclei [26]. A key point of this formalism is the calculation of the S matrix, which is determined from the choice of the neutron-target optical potential. In the transfer to the continuum method, this matrix is calculated for each different neutron final energy, obtaining an energy-dependent S matrix, which is best given by an energy-dependent optical potential, such as that used for the present calculations [12]. The first term of Eq. (1), proportional to $|1 - \bar{S}_{j_f}|^2$, gives the neutron elastic breakup spectrum, whereas the second term proportional to $1 - |\bar{S}_{j_f}|^2$ gives the neutron absorption spectrum. The absorption is due to resonant and nonresonant states of the neutron plus target continuum.

The cross section is calculated within a semiclassical model by an integration over the core-target impact parameter,

$$\frac{d\sigma_{1n}}{d\varepsilon_f} = C^2S \int_0^\infty b\, db \frac{dP(b)}{d\varepsilon_f} P_{el}(b), \quad (2)$$

where $dP/d\varepsilon_f$ is given by Eq. (1), C^2S is the spectroscopic factor of the neutron single-particle initial state, and $P_{el}(b)$ is the core survival probability in the elastic channel. The latter is parametrized in terms of the S matrix for the core-target scattering as [32]

$$P_{el}(b) = |S_{cT}|^2 = e^{(-\ln 2e^{(R_s - b)/\Delta})}. \quad (3)$$

This is possible since the conditions for the semiclassical approximation to the relative ion-ion scattering apply to the reaction discussed in this paper (Sommerfeld parameter $\eta = 2.33$). The strong absorption radius is defined as $R_S = 1.4(A_P^{1/3} + A_T^{1/3})$ in femtometers, and $\Delta = 0.6$ fm is a diffusenesslike parameter. The total breakup cross section is then obtained from Eq. (2) by integrating over the final neutron continuum energy ε_f. Equation (3) corresponds to a smooth cutoff model for the ejectile-target scattering, and its expression ensures that at an impact parameter b equal to the strong absorption radius R_s, the ejectile-target elastic scattering probability reduces to $\frac{1}{2}$.

V. POTENTIALS USED IN THE CALCULATION

The calculations need the knowledge of both initial and final single-particle states of the transferred neutron. The initial state is bound in the projectile, and the final states are unbound with respect to the target.

To obtain the radial wave functions of the initial (projectile) bound states and the corresponding asymptotic normalization constant C_i, the Schrödinger equation has been solved numerically by fitting the depths of the Woods-Saxon potentials V_0 to the experimental separation energies S_n. It is known that ^{18}O$_{\text{g.s.}}$

TABLE I. Parameters used for the ^{18}O potential.

	S_n (MeV)	V_0 (MeV)	R_0 (fm)	a_0 (fm)	V_{SO} (MeV)	R_{SO} (fm)	a_{SO} (fm)	C_i(fm$^{-1/2}$)	S^a
g.s. ($1d_{5/2}$)	8.044	62.7	2.91	0.56	5.5	2.96	0.5	1.73	0.759
g.s. ($2s_{1/2}$)	8.044	72.9	2.91	0.56	5.5	2.96	0.5	6.02	0.135

[a]From Ref. [3].

wave function contains an admixture of $(1d_{5/2}{}^2)_0$(∼75.9%) and $(2s^2_{1/2})_0$(∼13.5%) configurations [3]. As a consequence, the presence of peaks corresponding to the excitation of the ^{17}O first excited state can be taken into account in the calculation that considers the removal of the neutron from the $2s_{1/2}$ orbital. The parameters which were used to fit the separation energy for $^{18}O_{g.s.}$ have been calculated for both $1d_{5/2}$ and $2s_{1/2}$ orbitals as listed in Table I. The neutron separation energies are the same since the two configurations are degenerate in $^{18}O_{g.s.}$.

It is interesting to note that the asymptotic normalization constants C_i, reported in Table I for both configurations, are consistent with those used in Ref. [33] for recent calculations of reaction rates for astrophysical processes that involve the same oxygen isotopes we are studying here.

The potentials used to calculate the energy-dependent S matrix are the n-^{9}Be optical-model potentials recently developed by two methods in Ref. [12]. In one case (AB), the authors started from the potential of Refs. [34,35] and extended it to the full range of incident neutron energies for which experimental data are available (i.e., from ∼0.5 to ∼50 MeV). The phenomenological AB potential is

$$U_{AB}(r,E) = -[V_{\rm WS}(r,E) + \delta V(r,E) + i\,W_{AB}(r,E)], \quad (4)$$

which contains a Woods-Saxon real volume and spin-orbit term ($V_{\rm WS}$), a correction δV necessary to take into account the surface-deformation effects, and an imaginary term (W_{AB}) that consists of both surface and volume components. The second method used in Ref. [12] is the dispersive optical model (DOM) where there is a contribution to the real potential that arises from the imaginary potential via a dispersion relationship. Both potentials reproduce the experimental cross section at all energies, in particular, the $p_{3/2}$ resonance at $E_{\rm lab} = 0.7$ MeV and the $d_{5/2}$ resonance at $E_{\rm lab} = 3.1$ MeV. In the present calculations, both potentials are used to calculate the phase shift and the S matrix needed by the formalism to perform the one-neutron transfer to the continuum in the ^{18}O + ^{9}Be reaction, and a comparison between the two results is made.

VI. DATA ANALYSIS

To perform a calculation which can be compared to the experimental data, a correspondence between the scattering angle θ and the impact parameter b is needed. The functional relation $\theta = \theta(b)$ has been computed according to Ref. [36], thus making a correspondence of the range $3^\circ < \theta_{\rm lab} < 10^\circ$ to $6.8 < b < 7.8$ fm. The results obtained by using this approach are superimposed on the experimental continuum spectrum of ^{10}Be in Fig. 3(a) by using the DOM potential and in Fig. 3(b) by using the AB potential. The elastic breakup (red-dashed-dotted curve) and the absorption (blue-dotted curve) components are shown as given by the first and second terms of Eq. (1),

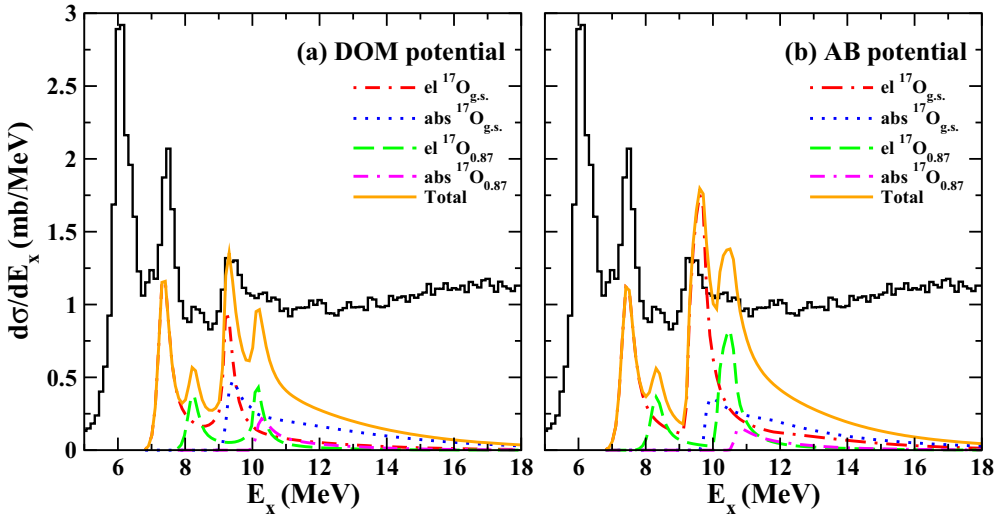

FIG. 3. (Color online) Inclusive excitation energy spectrum of the reaction for $3^\circ < \theta_{\rm lab} < 10^\circ$ and theoretical calculations of various breakup components (see text) that use: (a) the DOM potential and (b) the AB potential. In both panels, the red-dotted-dashed (el $^{17}O_{g.s.}$) and blue-dotted (abs $^{17}O_{g.s.}$) curves represent the elastic and the absorption breakups that correspond to the emission of a neutron which leaves the ^{17}O in its ground state. The green dashed curve (el $^{17}O_{0.87}$) and the pink double-dashed-dotted curve (abs$^{17}O_{0.87}$) represent the elastic and the absorption breakups that correspond to the ^{17}O core in its first excited state at 0.87 MeV. The orange curve (total) is the sum of all contributions. All calculations are folded with the experimental resolution.

respectively. These are relative to the emission of a neutron which leaves ^{17}O in its ground state. The calculations include the spectroscopic factor S indicated in Table I, which comes from the estimates of the configuration mixing in the $^{18}O_{g.s.}$ wave function [3].

To describe the peaks in the experimental spectra that come from the transition which leaves the ^{17}O core in its first excited state at 0.87 MeV, supplementary calculations in which the ^{18}O neutron is emitted from the $2s_{1/2}$ orbital have been performed. The resulting energy spectrum of the scattered neutron is shifted by 0.87 MeV, and it includes the spectroscopic factor S (as listed in Table I) according to the shell-model configuration admixtures in the ^{18}O ground-state wave function [3]. It is worth noticing that the spectroscopic factor is also consistent with the experimental ratio ($\sim$0.2) between the $^{10}Be_{g.s.}(^{17}O_{g.s.})$ and the $^{10}Be^{*}_{g.s.}(^{17}O_{0.87})$ yields, deduced from the experimental spectrum shown in Fig. 1. The results are superimposed on the experimental spectrum in Fig. 3 (green-dashed and pink-double-dashed-dotted curves for elastic breakup and absorption, respectively). The sums of all four contributions are shown by the orange curves. Both optical potentials reproduce the ^{10}Be continuum spectrum reasonable well, without need of any scaling factor. In particular, two ^{10}Be single-particle resonances are reproduced, one at $E_x = 7.54$ MeV, built mainly as $|^9Be_{g.s.}(3/2^-) \otimes (1p_{1/2})_v\rangle$ and at $E_x = 9.27$ MeV, which shows a dominant $|^9Be_{g.s.}(3/2^-) \otimes (1d_{5/2})_v\rangle$ configuration. These configurations have been identified by looking at the contribution of each single partial wave j_f to the total sum. This is possible since Eq. (1) contains an incoherent sum over final angular momenta. The partial-wave decomposition of the theoretical energy spectrum obtained by using the DOM potential [Fig. 3(a)] is shown in Fig. 4. The spectrum is dominated by the two resonances at 7.54 and 9.27 MeV, which correspond to the $p_{1/2}$ (red curve) and $d_{5/2}$ (blue-dashed curve) orbitals, respectively. The contribution of other partial waves to the total cross section is found to be negligible. The partial-wave decomposition that corresponds to the use of the AB potential presents the same dominant components. Here we point out that the possibility to calculate very accurately the strength distribution of each partial wave via the transfer to the continuum method provides an unambiguous way to determine the angular momentum of the resonances. This approach goes well beyond the traditional DWBA method of fitting an angular distribution whose measurement is not necessary for final continuum states when heavy nuclei are involved. Indeed, when considering final continuum states populated by heavy-ion reactions, the angular distributions are featureless as is well known and already seen in Ref. [3] because, at any energy, all angular momenta contribute. This phenomenon is observed also in the present case by comparing spectra taken at three different angles in the energy range $5 < E_x < 13$ MeV, shown in Fig. 5. The only difference in the three cases is a scaling in the absolute value of the cross section, which decreases with increasing angles. Contrary to the (d,p) cases, for heavy ions the core-target scattering is characterized by strong absorption, which washes out diffraction oscillations. For this reason it is possible to calculate the cross section as an integral over impact parameters, which means assuming a simple classical relationship between angle

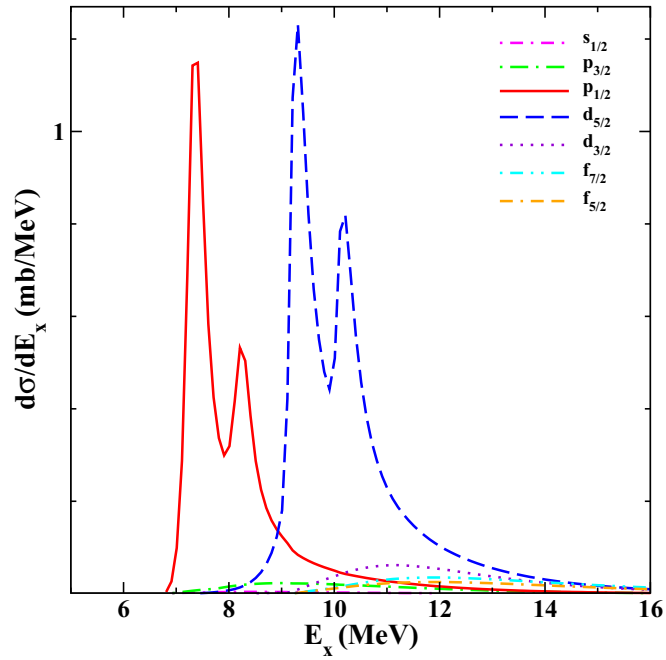

FIG. 4. (Color online) Dominant contributions to the partial-wave decomposition of the theoretical energy spectrum shown in Fig. 3(a). The legend indicates the single-particle angular momentum of each individual strength distribution.

and impact parameter and thus a smooth decrease in the cross section with increasing angle. Indeed, in our case the grazing angle is $\theta_c = 4.8^\circ$, and data corresponding to $5.5^\circ < \theta_{CM} < 9.5^\circ$ are shown in Fig. 5. It is clear that, in this condition, the angular distributions would never provide unambiguous information about the angular momentum populated. On the contrary, by using the present transfer to the continuum model, the determination of the angular momentum and spin of the resonances are absolutely unambiguous thanks to the fact that Eq. (1) contains an incoherent sum over final partial waves. The strength distribution of each of them is provided by the energy dependence of the optical potential used in the n-^{9}Be S matrix.

It is interesting to point out that there are some differences between the cross section that results from the present calculations and that obtained in Ref. [12], even though the same potentials were used. One has to do with the order of magnitude of the cross section, which is much reduced in the present case (order of millibarns) because of the rescattering of the neutron emitted by the ^{18}O projectile compared to the scattering of a free neutron in the n-^{9}Be calculation of Ref. [12]. This aspect influences also the ratio between the two resonances appearing in the calculated cross section, indeed the $d_{5/2}$ resonance is more populated than the $p_{1/2}$ resonance because the emitted neutron belongs to the sd shell in ^{18}O. The ratio of the strength of the two resonances was opposite in the case of free scattering [12]. This effect is due to the matching of angular momentum and spin as described in Ref. [30].

Resonances at $E_x = 7.37(3^-), 9.4(2^+)$ MeV are not reproduced within the present approach because they are built on

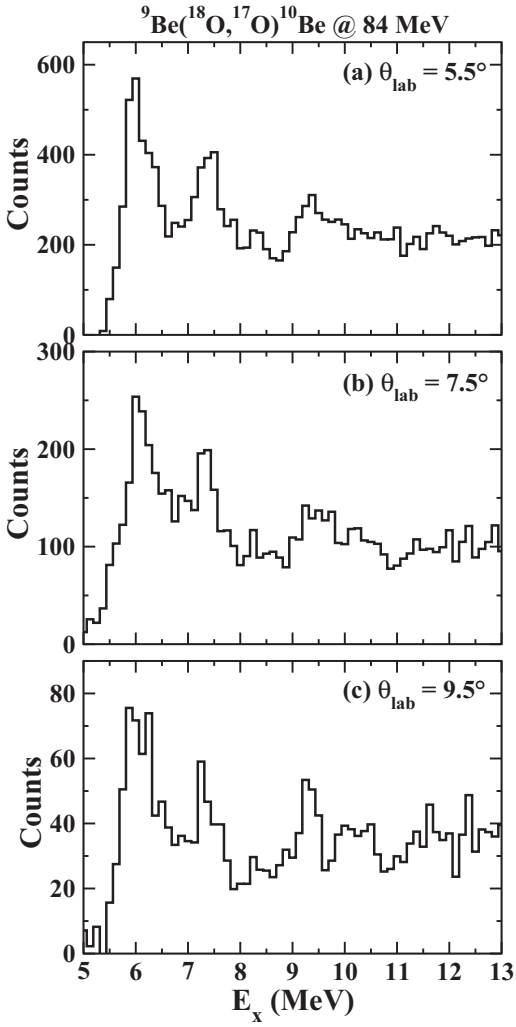

FIG. 5. Excitation energy spectra of the ^{9}Be(^{18}O,^{17}O)^{10}Be reaction at 84-MeV incident energy for (a) $\theta_{\rm lab} = 5.5^{\circ}$; (b) $\theta_{\rm lab} = 7.5^{\circ}$; (c) $\theta_{\rm lab} = 9.5^{\circ}$. The background that comes from ^{12}C and ^{16}O impurities has been subtracted.

more complicated configurations which are not included in the transfer to the continuum model.

A comparison of the calculations obtained by using the AB and the DOM potentials is visible in Fig. 2 in which the total theoretical energy spectra are superimposed on the experimental one. The two calculations are almost identical in their description of the resonance at 7.54 MeV, whereas the DOM potential describes better the region of the resonance at 9.27 MeV, both in energy and in the absolute value. At higher excitation energies above 11 MeV, both calculations give a very small contribution to the inclusive experimental spectrum, which shows an almost flat behavior. Other contributions are expected there since the two-neutron ($S_{2n} = 8.476$ MeV) and α ($S_{\alpha} = 7.409$ MeV) emission thresholds are opening. To estimate these contributions, at least their shapes, the experimental data [22] of ^{9}Be(n,nn)^{8}Be [23] and ^{9}Be(n,α)^{6}He [24] are superimposed on the experimental spectrum in Fig. 2. The data have been scaled by a factor of 10^{-3} that results from the ratio between the free n-^{9}Be cross section [12] and the present ^{18}O-^{9}Be reaction. As expected, these breakup channels manifest a shape compatible with the flat background above 11 MeV in the present experimental ^{10}Be spectrum. These contributions should be consistently added to our calculations through a model that contains the correct kinematics for all channels. The calculation of these contributions is beyond the scope of the present paper, and it is not available at the present stage of theory.

VII. CONCLUSIONS

In this paper we have reported the results of the (^{18}O,^{17}O) reaction on ^{9}Be at 84 MeV of incident energy. Below the S_n threshold, the cross section is concentrated in several ^{10}Be bound states. Above S_n, two narrow peaks are identified, which correspond to the superposition of the resonances at $E_x = 7.37(3^-), 7.54(2^+)$ MeV and at $E_x = 9.27(4^-), 9.4(2^+)$. Each ^{10}Be state shows up as a doublet that corresponds to the ^{17}O ejectile emitted in its ground and first excited states at $E_x = 0.87(1/2^+)$ MeV. In the energy region above 10 MeV, a large background is observed.

Both the elastic breakup and the absorption channels have been analyzed in a consistent way. In the adopted theoretical model, the interaction of the neutron, removed from the ^{18}O projectile with the target nucleus, is described by means of an optical potential with a semiclassical approximation for the relative motion. We present and compare the results obtained using two parametrizations (DOM and AB) of the optical-model potential for the system n-^{9}Be over a large energy range, which were successfully employed to describe the free n-^{9}Be scattering.

The ^{10}Be continuum spectrum is reproduced quite well by both parametrizations, which include the spectroscopic factors known in literature, without the need of any other scaling factors. The theoretical spectrum is dominated by two single-particle resonances at $E_x = 7.54, 9.27$ MeV, which correspond to the $p_{1/2}$ and $d_{5/2}$ orbitals, respectively. The DOM optical potential is found to describe better the absolute cross section and the resonance energies. The absolute values of the two theoretical cross sections differ by $\sim$35%, which can be compared to the experimental uncertainty ($\sim$10%). In particular, the main difference between the two calculations is found in the region of the resonance at $E_x = 9.27$ MeV. The DOM potential describes well the centroid ($E_x^{\rm DOM} \sim 9.3$ MeV) and the absolute cross section, whereas the AB one overestimates the absolute cross section and exhibits a centroid $E_x^{AB} \sim 9.6$ MeV. This effect is due to the different ratios of elastic and reaction cross sections in the $d_{5/2}$ resonance region, which in turn comes from the different real and imaginary parts in the two optical potentials. It is very interesting that such differences would show up in the transfer calculation, whereas the free-particle cross sections were almost undistinguishable. It is therefore proof that great care has to be taken in extracting a neutron-nucleus potential from reactions, such as (d,p), used to populate resonances of unbound exotic nuclei.

Finally, the higher part of the ^{10}Be continuum contains other contributions not included in the present model, which probably correspond to the ^{9}Be(n,nn)^{8}Be and ^{9}Be(n,α)^{6}He breakup channels.

The successful description of the ^{10}Be continuum populated by the (^{18}O,^{17}O) reaction could have a strong impact on the study of the ^{11}Be nucleus populated via the (^{18}O,^{16}O) reaction at the same incident energy. Indeed, the ^{9}Be(^{18}O,^{17}O)^{10}Be reaction represents the important intermediate channel for an independent removal description of the two-neutron transfer reaction.

ACKNOWLEDGMENTS

The work of one of us (D.C.) was supported by the Italian Ministry of Education, Universities and Research (MIUR) under the grant "LNS-Astrofisica Nucleare (fondi premiali)." The work of R.J.C. was supported by the US Department of Energy, Office of Science, Office of Nuclear Physics under Award No. DE-FG02–87ER-40316.

[1] N. Anyass-Weiss *et al.*, Phys. Rep. **12**, 201 (1974).
[2] S. Kahana and A. J. Baltz, Adv. Nucl. Phys. **9**, 1 (1977).
[3] M. Cavallaro *et al.*, Phys. Rev. C **88**, 054601 (2013).
[4] G. R. Satchler, *Direct Nuclear Reactions* (Oxford University Press, New York, 1983).
[5] DREB (2014) https://indico.gsi.de/conferenceTimeTable.py?confId=2347#20140630
[6] A. Bonaccorso, I. Lhenry, and T. Suomijärvi, Phys. Rev. C **49**, 329 (1994).
[7] A. Bonaccorso, Phys. Rev. C **51**, 822 (1995).
[8] F. Cappuzzello *et al.*, Phys. Lett. B **711**, 347 (2012).
[9] D. Carbone *et al.*, EPJ Web of Conferences **66**, 03015 (2014).
[10] D. Carbone *et al.*, Acta Phys. Pol. B **45**, 431 (2014).
[11] H. Knoth *et al.*, Nucl. Phys. A **172**, 25 (1971).
[12] A. Bonaccorso and R. J. Charity, Phys. Rev. C **89**, 024619 (2014).
[13] A. Cunsolo *et al.*, Nucl. Instrum. Methods Phys. Res., Sect. A **481**, 48 (2002).
[14] A. Cunsolo *et al.*, Nucl. Instum. Methods Phys. Res., Sect. A **484**, 56 (2002).
[15] M. Cavallaro *et al.*, Eur. Phys. J. A **48**, 59 (2012).
[16] F. Cappuzzello *et al.*, Nucl. Instrum. Methods Phys. Res., Sect. A **621**, 419 (2010).
[17] F. Cappuzzello *et al.*, Nucl. Instrum. Methods Phys. Res., Sect. A **638**, 74 (2011).
[18] M. Cavallaro *et al.*, Nucl. Instrum. Methods Phys. Res., Sect. A **637**, 77 (2011).
[19] R. E. Anderson *et al.*, Nucl. Phys. A **236**, 77 (1974).
[20] S. E. Darden *et al.*, Nucl. Phys. A **266**, 29 (1976).
[21] G. Blanchon, A. Bonaccorso, and N. Vinh Mau, Nucl. Phys. A **739**, 259 (2004).
[22] EXFOR nuclear data library http://www-nds.iaea.org/exfor/exfor.htm
[23] I. Murata *et al.*, *International Conference on Nuclear Data for Science and Technology, Nice, 2007* (EDP Sciences, LesUlis, France, 2007), Vol. 2, p. 999; D. M. Drake *et al.*, Nucl. Sci. Eng. **63**, 401 (1977); H. C. Catron *et al.*, Phys. Rev. **123**, 218 (1961); G. J. Fischer, *ibid.* **108**, 99 (1957).
[24] R. Bass, T. W. Bonner, and H. P. Haenni, Nucl. Phys. **23**, 122 (1961); P. H. Stelson and F. C. Campbell, Phys. Rev. **106**, 1252 (1957); M. E. Battat and F. L. Ribe, *ibid.* **89**, 80 (1953).
[25] A. Bonaccorso and D. M. Brink, Phys. Rev. C **38**, 1776 (1988).
[26] A. Bonaccorso and D. M. Brink, Phys. Rev. C **43**, 299 (1991).
[27] A. Bonaccorso and D. M. Brink, Phys. Rev. C **44**, 1559 (1991).
[28] A. Bonaccorso and D. M. Brink, Phys. Rev. C **46**, 700 (1992).
[29] L. Lo Monaco and D. M. Brink, J. Phys. G **11**, 935 (1985).
[30] A. Bonaccorso, D. M. Brink, and L. Lo Monaco, J. Phys. G **13**, 1407 (1987), and references therein.
[31] H. Hashim and D. M. Brink, Nucl. Phys. A **476**, 107 (1988).
[32] A. Bonaccorso, Phys. Rev. C **60**, 054604 (1999).
[33] T. Al-Abdullah *et al.*, Phys. Rev. C **89**, 025809 (2014).
[34] J. H. Dave and C. R. Gould, Phys. Rev. C **28**, 2212 (1983).
[35] A. Bonaccorso and G. F. Bertsch, Phys. Rev. C **63**, 044604 (2001).
[36] R. A. Broglia and A. Winther, *Heavy-Ion Reactions* (Addison-Wesley Publishing Company, Redwood City, California, 1991).